喷涂工艺参数对硅灰石涂层结构的影响

黄 青, 王卫泽, 万 雷, 轩福贞*
(华东理工大学 承压系统安全科学教育部重点实验室, 上海 200237)

摘 要: 采用等离子喷涂方法, 在不同喷涂距离、主气流量和喷涂功率下制备硅灰石涂层. 使用扫描电镜观察了涂层的微观形貌, 研究了喷涂工艺参数对涂层结构的影响. 结果表明, 在较大主气流量下, 随着喷涂距离增加, 涂层粒子扁平化程度降低, 涂层内孔隙逐渐增多; 在较小主气流量下, 涂层粒子扁平化程度随喷涂距离增加呈现先增加后减小的趋势. 主气流量增加, 涂层致密, 粒子扁平充分. 喷涂功率增加, 粒子熔化好, 涂层致密; 但随喷涂功率进一步增加, 涂层中出现较多的圆形孔隙. 喷涂工艺参数对涂层结构的影响主要通过影响熔融粒子的温度和速度所致.

关键词: 等离子喷涂; 硅灰石涂层; 喷涂距离; 喷涂功率; 气体流量
中图分类号: TG174 文献标识码: A 文章编号: 0253-360X(2010)03-0045-04


黄 青

0 序 言

等离子喷涂羟基磷灰石(HA)涂层已经广泛用作人工骨植入材料. 但是其结晶度较低, 从而造成涂层的早期溶解和降解, 影响植入物的效果. 所以从材料学角度, 近年来有很多研究是针对提高HA涂层结晶度展开的[1-3]. 但是附加的处理工艺使得生物涂层的制备工艺变得更加复杂, 同时HA涂层与钛合金基体的结合强度较低, 只有二十几兆帕.

等离子喷涂硅灰石涂层具有良好的细胞相容性和成骨诱导能力, 且结合强度可以达到39 MPa, 约为常用的羟基磷灰石涂层结合强度的二倍, 因此被认为是极具应用前景的生物医学材料[4]. 但等离子喷涂是一个复杂的工艺过程, 涂层性能受到多个参数的影响, 如喷涂工艺、喷涂粉末的形状、尺寸等. 为得到高质量的硅灰石涂层, 使用大气等离子喷涂设备, 在不同的喷涂距离、主气流量及喷涂功率下制备了硅灰石涂层, 并研究了这三个工艺参数对涂层结构的影响规律, 为选择最佳制备工艺提供依据.

1 喷涂材料与工艺

试验所用材料是粒径为-325目的硅灰石粉末(图1a), 粉末的微观结构主要呈短纤维状. 喷涂设备为北京航空工艺研究所生产APS—2000型等离子喷涂系统. 试验主气为氩气, 辅助气体为氢气, 送粉气体为氩气. 主气压力为0.4 MPa, 辅助气体压力为0.25 MPa. 在不同喷涂距离(80, 100和120 mm)、喷涂功率(33, 36和39 kW)和主气流量(36和85 L/min)下制备硅灰石涂层. 喷涂前用80目棕刚玉进行喷砂粗化处理, 喷砂气体压力为0.6 MPa. 采用日本电子(JEOL)公司JSM—6360LV型扫描电子显微镜, 对等离子喷涂硅灰石涂层的微观结构进行观察.

2 结果与讨论

2.1 硅灰石粉末的球化处理

由于硅灰石粉末密度小, 且呈短纤维状的粉末易团聚、流动性差, 喷涂过程中原始粉末基本无法由送粉器(DPSF-2型)送出. 而球形粉末的比表面积最小, 各向受热均匀, 在等离子焰流的高温作用下, 其表面受热氧化及受其它杂质污染的程度比不规则粉末小, 因此热喷涂过程中粉末最好呈球形或近似球形. 为了提高粉末的流动性, 选用机械研磨法对粉末进行球化处理. 处理后的粉末形貌如图1b所示, 喷涂过程中球化处理后粉末的送粉情况良好.

2.2 喷涂距离对硅灰石涂层结构的影响

图2与图3分别是主气流量为85与36 L/min, 喷涂功率为36 kW时, 喷涂距离对等离子喷涂硅灰石涂层结构的影响. 从图2与图3均可以看出, 喷

收稿日期: 2008-09-19
基金项目: 国家自然科学基金资助项目(50805048); 上海市自然科学基金资助项目(08ZR1405700); 教育部新教师基金资助项目(200802511008); 上海市青年科技启明星计划(10QA1401500)

*参加此项目工作的还有涂善东教授

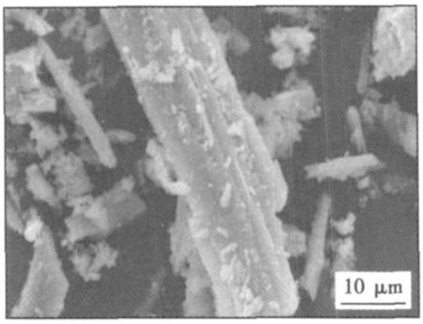

(a) 供货态

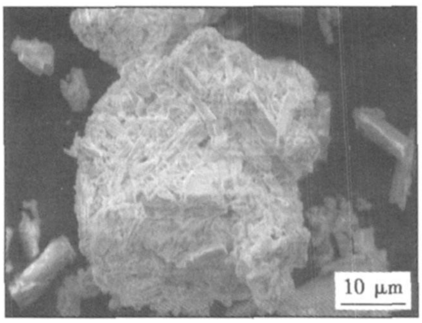

(b) 球化处理后

图 1 硅灰石粉末形貌

Fig. 1 Morphology of wollastonite powders

涂距离是影响涂层结构的重要参数. 当主气流量为 85 L/min,喷涂距离为 80 mm时制备涂层的结构最致密,涂层内孔隙少,而随着喷涂距离增加,涂层内孔隙增多. 喷涂距离为 100 mm时制备涂层的粒子的扁平化程度略好于喷涂距离为 120 mm. 主气流量为 36 L/min,喷涂距离为 100 mm时涂层的扁平化程度最好. 喷涂距离为 80和 120 mm时,涂层中有许多未完全扁平化的球状粒子,各粒子之间结合不紧密,粒子与粒子之间有孔隙.

Madjeski[5]对等离子喷涂粒子撞击基体后形成扁平粒子的行为进行了研究,在忽略凝固对粒子扁平化影响的情况下,扁平粒子的大小由下式确定,即

$$\frac{3\xi^2}{W_e}+\frac{1}{R_e}\left(\frac{\xi}{1.29}\right)^2=1 \tag{1}$$

式中: $\xi=D/d$为粒子的扁平率; D为扁平后粒子的直径; d为喷涂粒子直径; $W_e=\rho v^2 d/\sigma$ 为韦伯数; ρ为熔滴密度; v为熔滴的初始碰撞速度; σ为熔滴的表面张力; $R_e=\rho dv/\eta$, η为熔滴的粘性系数. 在热喷涂条件下, $1/W_e\approx0$, 而且一般 $R_e>100$, 则上式简化为

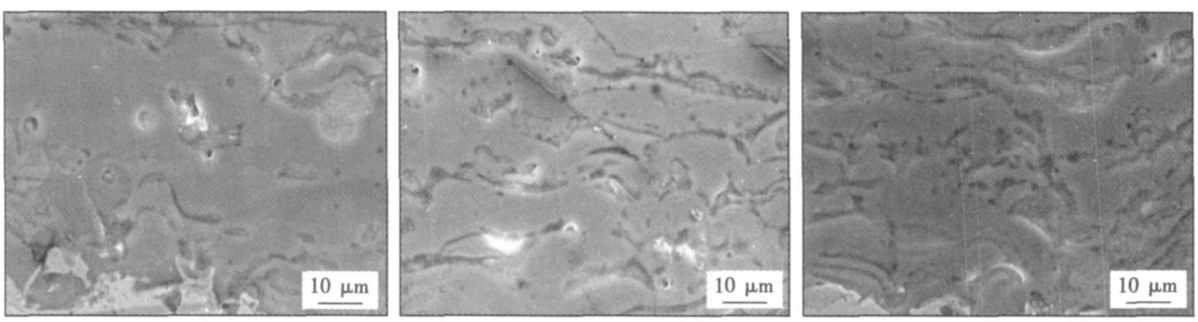

(a) 80 mm (b) 100 mm (c) 120 mm

图 2 喷涂距离对等离子喷涂硅灰石涂层结构的影响(电弧功率 36 kW,主气流量 85 L/min)

Fig. 2 Effect of spraying distance on microstructure of plasma sprayed wollastonite coatings (plasma power 36 kW, primary gas flow rate 85 L/min)

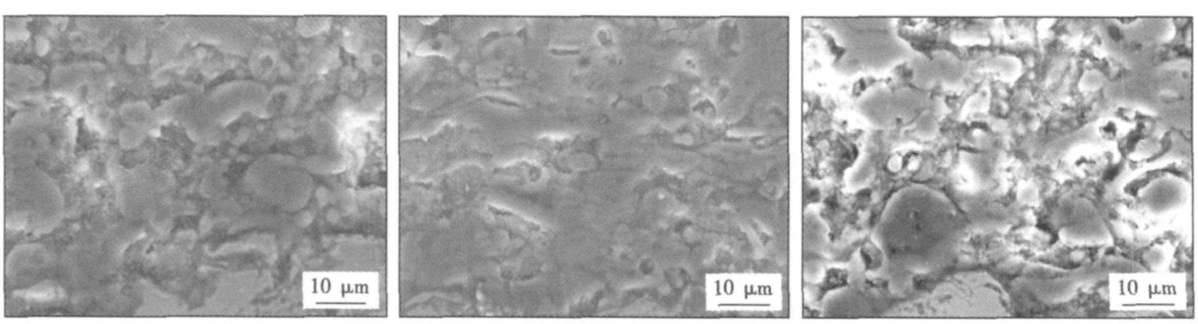

(a) 80 mm (b) 100 mm (c) 120 mm

图 3 喷涂距离对等离子喷涂硅灰石涂层结构的影响(电弧功率 36 kW,主气流量 36 L/min)

Fig. 3 Effect of spraying distance on microstructure of plasma sprayed wollastonite coatings (plasma power 36 kW, primary gas flow rate 36 L/min)

$$\xi = 1.29\left(\frac{\rho d v}{\eta}\right)^{0.2} \quad (2)$$

可见,熔滴的速度越大、粘性系数越小,则扁平后的粒子直径越大,即粒子扁平越充分.

根据等离子喷涂中氧化铝陶瓷粒子温度、速度随喷涂距离变化的测量结果[6],随喷涂距离增加,粒子的温度与速度均呈先升高后降低的趋势. 温度升高或降低将导致粒子的粘性系数相应减小或增加,而粘性系数增加,不利于熔化粒子对已形成的涂层表面的填充,在涂层层间易于形成孔隙. 因此随喷涂距离的增加,粘性系数和粒子速度的变化将共同影响喷涂粒子的扁平化程度与粒子间的结合状态.

喷涂主气流量为 85 L/min时,随喷涂距离增加,涂层内孔隙逐渐增多,且层间未结合间隙的宽度增加. 这与喷涂距离增加,粒子速度与温度的降低有关. 根据上面的分析,粒子温度降低,粘性系数增加,同时粒子速度的降低,使得熔化粒子的扁平化以及对形成涂层的填充降低,因此形成随喷涂距离增加,涂层微观结构中孔隙增多的趋势. 而喷涂主气流量为 36 L/min时,随喷涂距离增加,粒子的扁平化程度逐渐增加,之后随喷涂距离继续增加,扁平化程度降低. 这与喷涂距离增加,粒子的速度与温度先升高后降低有关. 另外当主气流量增加时,粒子温度与速度达到最大值所对应的喷涂距离缩短.

2.3 喷涂主气流量对硅灰石涂层结构的影响

由图 2和图 3可见,当主气流量增加时,涂层结构更致密,涂层中孔隙少,粒子扁平化程度增加. 假设射流为一维流动且流动速度恒定,粒子运动轨迹与流体流动方向一致,不计重力的影响,并且粉末颗粒浓度足够小,即忽略粒子对等离子射流的负载效应,并假设粉末粒子之间不发生相互作用,粒子的存在也不影响流体的热力学性质时,得到粒子的运动方程[7]为

$$\frac{\partial v_p}{\partial t} = \frac{3}{4}\frac{\rho_f}{\rho d} C_D \left| v_f - v_p \right| (v_f - v_p) \quad (3)$$

式中:下标 f代表流体; C_D为拖曳系数. 可见流体速度越大,粒子的速度越大,且达到相同速度所需的时间越短. 因此当主气流量增大时,硅灰石粒子达到的最大速度更大,达到最大速度所需时间更短. Geessasma等人[8]对氧化铝—氧化钛粒子的速度进行测量,结果表明当等离子气流量由 30 L/min增加到 50 L/min时,粒子速度由 186 m/s增加到 269 m/s,粒子速度增加明显. Fang等人[9]研究了主气流量对氧化锆粒子速度的影响,结果同样表明随主气流量增加,粒子的速度增大.

粒子速度增加,则粒子的扁平化程度增加,因此随主气流量增加,硅灰石涂层表现出层间结合紧、孔隙少的微观形貌. 而主气流量增加,粒子在较小的喷涂距离就可以达到最大喷涂速度,使得喷涂熔化粒子在较短的喷涂距离就可以充分扁平. 因此主气流量为 85 L/min,喷涂距离 80 mm时制备涂层较致密;而主气流量降低为 36 L/min,喷涂距离增加到 100 mm时涂层较致密.

主气流量增加,流速增大,喷涂粉末在等离子焰流中的停留时间减少,则粉末的加热效果受到一定影响,提高主气流速会降低粒子温度[9]. 但从图 2与图 3中涂层的微观结构看,主气流速增加,粒子温度降低对涂层结构影响的效果不明显. 这可能是由于主气流速增加,导致的粒子速度增加对涂层结构产生的影响,比粒子温度降低产生的影响更大所致.

2.4 喷涂功率对硅灰石涂层结构的影响

图 4是喷涂距离与主气流量保持不变时,在不同的喷涂功率下制备的硅灰石涂层的微观结构. 由图 4可见,当喷涂功率为 33 kW时,喷涂粒子熔化不好,涂层微观结构上可见大量的未熔粒子团聚形

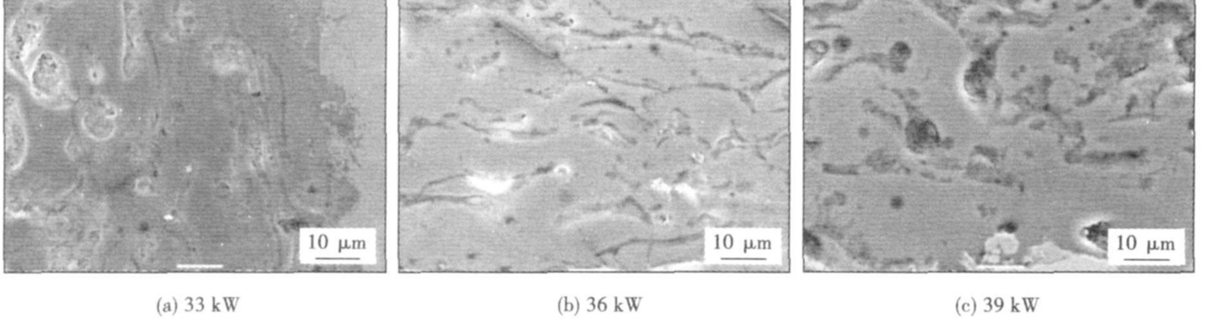

(a) 33 kW (b) 36 kW (c) 39 kW

图 4 喷涂功率对等离子喷涂硅灰石涂层结构的影响(主气流量 85 L/min,距离 100 mm)

Fig. 4 Effect of plasma power on microstructure of plasma sprayed wollastonite coatings (primary gas flow rate 85 L/min, spraying distance 100 mm)

貌. 随喷涂功率增加到 36 kW, 粒子扁平良好, 涂层内有结合区域与垂直裂纹. 随喷涂功率进一步增加到 39 kW, 涂层中可见不同尺寸的圆形孔洞, 且层间未结合孔隙宽度增加.

喷涂过程中熔融颗粒的速度、温度和粒子的直径是影响涂层形貌的因素. 随喷涂功率增加, 喷涂粉末的熔化程度越好, 熔融粒子的粘性系数越小, 则粒子扁平充分. 因此喷涂功率为 36 kW时制备的涂层结构致密, 而喷涂功率为 33 kW则不能使喷涂粉末充分熔化. 喷涂功率进一步增加, 喷涂粒子温度随之增加, 当粒子温度高于沸点时, 粒子的沉积效率反而会下降[9]. Dyshlovenko等人[10]的研究证明当喷涂电弧功率增加后, 单个扁平粒子的形貌由饼状转为花状, 同时在粒子中有大量的孔隙. 这与研究中喷涂功率进一步增加后观察到的涂层形貌一致.

3 结 论

主气流量由 36 L/min增加到 85 L/min时, 涂层结构更致密, 粒子扁平化程度更高. 随喷涂电弧功率增加, 涂层粒子熔化与扁平良好, 而电弧功率进一步增大时, 涂层中圆形孔隙增多. 喷涂工艺参数对涂层结构的影响, 主要影响熔融粒子的飞行速度与温度.

参考文献:

[1] Tao S Y, Ji H, Ding C X. Effect of vapor flame treatment on plasma sprayed hydroxyapatite coatings[J]. J Biomed Mater Res, 2000, 52(3): 572-575.

[2] Yang C W, Lee T M, Lui T S, et al. Effect of post vacuum heating on the microstructural feature and bonding strength of plasma-sprayed hydroxyapatite coatings[J]. Materials Science and Engineering C, 2006, 26(8): 1395-1400

[3] Dyshlovenko S, Pierlot C, Pawlowski L, et al. Experimental design of plasma spraying and laser treatment of hydroxyapatite coatings[J]. Surface & Coatings Technology, 2006, 201: 2054-2060

[4] Ding C. Progress in plasma sprayed bioceramic coatings[C] // Thermal Spray 2007: Global Coating Solution. Ohio: ASM International, 2007: 401-404

[5] Madjski J. Solidification of droplets on a cold surface[J]. J Heat Mass Transfer, 1977, 19(9): 1009-1013.

[6] Vardelle A, Vardelle M, McPherson R, et al. Study of the influence of particle temperature and velocity distribution within a plasma jet on coating formation[C] // Zaat D J H. Proceedings of the 9th International Thermal Spray Conference. Hague: ASM International, 1980: 155-161.

[7] 鲁丁格. 气体—颗粒流基础[M]. 北京: 国防工业出版社, 1986

[8] Guessasma S, Montavon G, Coddet C. Velocity and temperature distributions of alumina-titania in-flight particles in the atmospheric plasma spray process[J]. Surface & Coatings Technology, 2005, 192(1): 70-76

[9] Fang J C, Xu W J, Zhao Z Y, et al. In-flight behaviors of ZrO_2 particle in plasma spraying[J]. Surface & Coatings Technology, 2007, 201(9-11): 5671-5675.

[10] Dyshlovenko S, Pawlowski L, Roussel P, et al. Relationship between plasma spray operational parameters and microstructure of hydroxyapatite coatings and powder particles sprayed into water[J]. Surface & Coatings Technology, 2006, 200(12-13): 3845-3855.

作者简介: 黄 青, 女, 1985年出生, 硕士. 主要从事生物涂层方面的研究工作.

Email: jxhuangq@163.com

University, Xi'an 710049, China). p 37-40

Abstract: A numerical calculation model with local refined mesh for laser deep penetration welding of titanium alloy is presented. A Rotatry-Gauss body heat source model was established to accurately describe the shape of keyhole and molten pool of the laser welded joint. The profile of keyhole and molten pool as well as the distribution of high gradient residual stresse are obtained. It is showed that the region of high stress locates in the keyhole region, and high gradient residual stress distributes in the other region of welded seam. The stresse gradient increases in the state of excessively high and low level of energy density as well as the state of lower linear energy. It is supposed that keeping the laser energy density in state of low and medium level or keeping the linear energy in state of low level could avoid the high gradient stresses.

Key words: high gradient residual stresses; energy density; linear energy; keyhole

Research on melting metal behavior of ultrasonic-tungsten inert gas welding SUN Qingjie, YANG Chunli, LIN Sanbao, FAN Yangyang (State Key Laboratory of Advanced Welding Production Technology, Harbin Institute of Technology, Harbin 150001, China). p 41-44

Abstract: The mechanism of melting behavior of metal under ultrasonic-tungsten inert gas (U-TIG) welding was studied. The results indicate that U-TIG welding can significantly enhance the arc force and electromagnetic convection, change the metal flow behavior, and increase the penetration and the ratio of depth to width. This method extends the application range and improves production efficiency of ordinary TIG welding. Besides, the mechanism of arc force enhancing and penetration increasing were also presented in combination with experiment and theoretical analysis.

Key words: ultrasonic-tungsten inert gas welding; arc force; arc shape; melting behavior

Effect of spray parameters on microstructure of plasma sprayed wollastonite coatings HUANG Qing, WANG Weize, WAN Lei, XUAN Fuzhen (Key Lab of Safety Science of Pressurized System, Ministry of Education, School of Mechanical and Power Engineering, East China University of Science and Technology, Shanghai 200237, China). p 45-48

Abstract: Wollastonite coating was prepared by plasma spraying at different spraying distances, primary gas flow rates and plasma power. The microstructure of the coating lager was examined by scanning electron microscope (SEM). The results show that the three spraying parameters affect the microstructure of wollastonite coatings greatly. Flatten degree of molten powder decreased and the number of pores increased with the increment of spraying distance at lager flow rate of primary gas. However, flatten degree of molten powder firstly increased and then decreased with the spraying distance at the lower flow rate of primary gas. The microstructure of coatings is denser with larger gas flow rate. Flatten degree increased with plasma power up to 36 kW. Further increase of plasma power results in more round pores appearing in coatings. Effect of spray parameters on the microstructure of wollastonite coatings mainly resulted from the influence on velocity and temperature of the molten droplets.

Key words: plasma spraying; wollastonite coating; spraying distance; plasma power; gas flow rate

Influence of transverse alternative magnetic field on microstructure and properties of plasma arc surfacing layer LIU Zhengjun, ZHAO Qian, SONG Xingkui, YANG Yang (School of Material Science and Engineering, Shenyang University of Technology, Shenyang 110870, China). p 49-52

Abstract: In the research of the influence of alternative pulsed magnetic field on microstructure and properties of nickel-base alloy, a transverse alternative pulsed magnetic field had been applied to the plasma arc surfacing welding on low carbon steel. The hardness, wear resistance and microstructure of surfacing layer with different pulsed magnetic field currents, duty cycles have been systematically analyzed. The results indicated that transverse alternative pulsed magnetic field can effectively improve the crystal shape of plasma arc surfacing layer, refine crystal grain. Proper pulsed magnetic field current, duty cycle can obtain the optimum effect on electromagnetic stirring, which can increase the amount of hardening phase in overlay deposit, control the growth direction of hardening phase and improve the hardness and wear resistance of the surfacing overlay.

Key words: plasma arc; transverse magnetic field; microstructure; wear resistance

Investigation on welding stress and strain of titanium alloy LI Ju[1], GUAN Qiao[1], SHI Yaowu[2] (1. Beijing Aeronautical Manufacturing Technology Research Institute, P. O. Box 863, Beijing 100024, China; 2. School of Material Science and Technology, Beijing University of Technology, Beijing 100022, China). p 53-56, 60

Abstract: The welding stress and strain were investigated using the finite element method combined with the experiments. The research results showed that the metal in the melting pool is melted in the frame of area with compressive plastic strain, and cooled down also in the frame of the area with compressive plastic strain. The tensile plastic strain is produced in the weld when it is in the state of 'mechanical melting' during the cooling process. But in the residual state, the compressive plastic strain still remains in the weld. The peak value of longitudinal tensile stress in the weld of titanium alloy is always lower than its yield strength at the appropriate temperature during the cooling process, this situation is kept until the residual state.

Key words: titanium alloy; welding; stress; strain

Finite element anlysis of welding sequence impact on blisk roundness ZHANG Xueqiu[1,3], YANG Jianguo[1,2], LIU Xuesong[1], CHEN Xuhui[1], FANG Hongyuan[1], QU Shen[2] (1. State Key Laboratory of Advanced Welding Production Technology, Harbin Institute of Technology, Harbin 150001, China; 2. Shenyang Liming Aero-Engine Group Corporation, Shenyang 110043, China; 3. Baosteel Group Corporation, Shanghai 201900, China). p 57-60

Abstract: The finite element model of blisk is made by the several softwares and based on the different temperature effects during the welding process, three kinds of typical welding